ACS APPLIED MATERIALS & INTERFACES

Research Article

www.acsami.org

# Inverted Planar Heterojunction Perovskite Solar Cells Employing Polymer as the Electron Conductor

Weiwei Wang, Jianyu Yuan, Guozheng Shi, Xiangxiang Zhu, Shaohua Shi, Zeke Liu, Lu Han, Hai-Qiao Wang,* and Wanli Ma*

Institute of Functional Nano and Soft Materials (FUNSOM), Soochow University, 199 Ren-Ai Road, Suzhou Industrial Park, Suzhou 215123, China

Supporting Information

**ABSTRACT:** Inverted planar heterojunction perovskite solar cells employing different polymers, poly{[*N*,*N*′-bis(2-octyldodecyl)-1,4,5,8-naphthalene diimide-2,6-diyl]-*alt*-5,5′-(2,2′-bithiophene)} (N2200), poly{[*N*,*N*′-bis(alkyl)-1,4,5,8-naphthalene diimide-2,6-diyl-*alt*-5,5′-di(thiophen-2-yl)-2,2′-(E)-2-(2-(thiophen-2-yl)vinyl)thiophene]} (PNVT-8), and PNDI2OD-TT as electron-transporting material (ETM) have been investigated for the first time. The best device performance was obtained when N2200 was applied as the ETM, with $J_{SC}$ of 14.70 mA/cm2, $V_{OC}$ of 0.84 V, and fill factor (FF) of 66%, corresponding to a decent power conversion efficiency (PCE) of ∼8.15%. Which is very competitive to the parameters ($J_{SC}$ 14.65 mA/cm2, $V_{OC}$ 0.83 V, FF 70%, and PCE 8.51%) of the reference device employing conventional PCBM as the ETM. The slightly lower FF could be mainly accounted for by the increased recombination in the polymer contained devices. This work demonstrated that polymeric materials can be used as efficient ETM in perovskite solar cells, and we believe this class of polymeric ETMs will further promote the performance of perovskite photovoltaic cells after extended investigation.

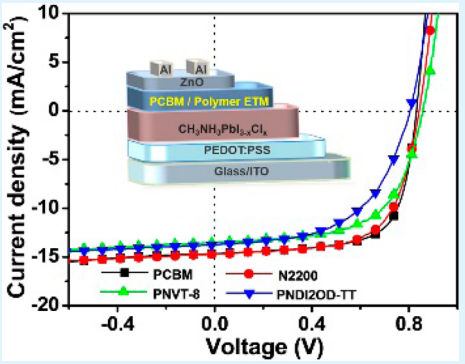


**KEYWORDS:** *planar heterojunction, perovskite solar cell, polymer, electron conductor, device performance, characterization*

## 1. INTRODUCTION

As light absorbers, compared to other conventional photovoltaic active materials, perovskite organo-lead halide compounds (e.g., $CH_3NH_3PbX_3$, X = I, Br, and Cl) possess the following advantages: direct optical band gap, broad range of light absorption extending over visible to near-infrared region,[1] and high extinction coefficient,[2] as well as low exciton bonding energy[3] and long diffusion length.[4,5] Moreover, organo-lead halide perovskite can behave in ambipolar characteristics for carrier transport and work well with organic carrier transporting materials to form a hybrid heterojunction (i.e., perovskite functions as "donor" material like in donor−acceptor polymer/organic planar and bulk-heterojunction solar cells) and generate an efficient photovoltaic effect.[6] Hence, organo-lead halide perovskite solar cells have shown promising performances[7−10] and are increasingly becoming the focus of photovoltaic research.

In 2009, Miyasaka et al.[11] pioneered the first perovskite solar cell based on mesoporous $TiO_2$ photoanode where the $CH_3NH_3PbX_3$ (X = I, Br) was used as sensitizer. Only moderate performance ($\eta$ = 3.81%) and poor stability of device were obtained due to the dissolution issues of perovskite in the electrolyte. To overcome the stability problem, in 2012, Park et al.[1] reported a new solid-state mesoscopic solar cell employing $(CH_3NH_3)PbI_3$ perovskite as the light absorber and spiro-MeOTAD film as the hole-transporting layer, and dramatically improved the device stability compared to the $(CH_3NH_3)PbI_3$-sensitized liquid[7] junction cells. With similar device fabrication, many efforts[7−9,12−16] mainly focused on the absorber layer, such as two-step process[7] and vapor deposition[8] have been reported, which led to high power conversion efficiency (PCE) over 15% and good reproducibility of planar heterojunction perovskite solar cells. In addition, at the beginning of 2014, solvent-engineering technology[17] was developed to form uniform and dense perovskite film, and PCE of 16.15% was certified for solution-processed perovskite solar cell. Very recently, by using modified ITO substrate and yttrium-doped $TiO_2$ as ETM, Yang et al.[18] achieved a new PCE record of ∼19.3%, with a planar geometry.

Since Park et al.[1] and Snaith et al.[19] reported the new solid-state mesoscopic perovskite solar cell in 2012, it has attracted great attention, achieved much progress, and shown great potential as a renewable energy strategy for real application. However, big issues are still there, and huge efforts are still needed to simplify the fabrication and further promote device performance and stability. For example, most of the above-mentioned perovskite devices require high temperatures (up to 500 °C) to sinter compact or mesoporous $TiO_2$ (or other similar metal oxides), which makes the fabricating process complicated and infeasible for flexible/plastic substrate. And the

**Received:** October 2, 2014
**Accepted:** January 30, 2015
**Published:** January 30, 2015





DOI: 10.1021/am506785k
*ACS Appl. Mater. Interfaces* 2015, 7, 3994−3999

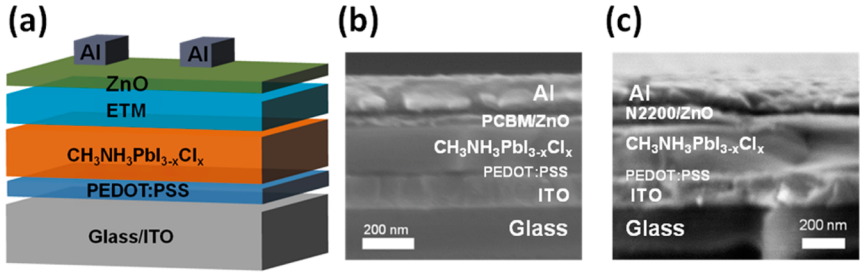


**Figure 1.** (a) Schematic of the inverted planar perovskite solar cell configuration consisting of a structure of ITO/PEDOT:PSS/$CH_3NH_3PbI_{3-x}Cl_x$/ETM/ZnO/Al. Cross-sectional SEM images of the optimized device configuration with (b) PCBM and (c) N2200 as ETM.

existence of mesoporous structure of the $TiO_2$ (or $Al_2O_3$ and ZrO) coated substrates can cause the pore-filling problem, which could degrade the performance, lower the stability and even damage the device.[8,19]

To overcome those issues for perovskite solar cells to approach the practical application target, some efforts have been made by researchers. As part of it, and inspired by the concepts, ideas, and achievements in OPV studies, in 2013, Jeng et al.[20] presented a hybrid perovskite solar cell using ITO/PEDOT:PSS substrate as the anode, a planar heterojunction (PHJ) $CH_3NH_3PbI_3$ perovskite/fullerene ($C_{60}$) as the active layer and aluminum as the cathode (which is later termed as inverted structure by Snaith[21]). Promising device performance with PCE of 1.6% was obtained, and which was elevated to 2.1 and 2.4% when PCBM and ICBA were used respectively to replace the fullerene as their higher lowest unoccupied molecular orbital (LUMO). It demonstrated the formation of the donor−acceptor interface at the $CH_3NH_3PbI_3$ perovskite/organic-material contact, and the modulation of the performance by varied LUMO levels of the acceptor. Almost at the same time, by using the similar architecture, Lam et al.[22] reported a PCE of 7.4%, with a sequential-deposition/two-step method fabricated perovskite film. After that, Snaith et al.[21] introduced a thin compact $TiO_x$ film to modify the interface between $PC_{61}BM$ and Al electrode and used $CH_3NH_3PbI_{3-x}Cl_x$ as the absorber, and achieved a high PCE of 9.8%. By coevaporating $PbI_2$ and MAI to prepare the perovskite film and inserting an electron blocking (polyTPD) layer between perovskite and PEDOT:PSS, Bolink et al.[10] pushed the PCE to 12% and with high open circuit voltage ($V_{OC}$) of 1.05 V. With similar device configuration, some other works focusing on the interface modification,[23] additives,[24,25] controlling of the growth and crystallization of perovskite,[26−29] and so on, have also delivered decent efficiencies over 10%. And very recently, even higher PCE (over 16%) for inverted perovskite solar cell has been achieved.[30]

However, until now, only a few organic small molecules, such as fullerene, PCBM and ICBA, have been demonstrated to be effective as ETMs in perovskite solar cells with this inverted/or similar architecture, which is still in a very beginning stage. Organic polymers, as far as we know, have never been used as ETM in such perovskite solar cells or with similar configurations, although huge amount of organic polymers as ETM or acceptor in organic solar cell have been confirmed and excellent results have been achieved. Given the abundant acceptor polymer materials, their easy tunable properties, flexible fabrication processes, and potential ability to generate extra current density for perovskite solar cell, it is worth exploring and making use of ideal polymeric materials as ETM in perovskite solar cells to promote the perovskite solar cell technology.

In the present work, we introduce polymer N2200 as the ETM in inverted solid state hybrid perovskite solar cells employing $CH_3NH_3PbI_{3-x}Cl_x$ as the light absorber and PEDOT:PSS as the hole-transporting material (HTM). As polymer N2200 possesses high electron mobility, strong light absorption extending to near-infrared regime[31] and compatible HOMO/LUMO levels to the perovskite.[32−34] The obtained perovskite solar cells display fair performances, with PCE over 8% and even approaching 9%, under simulated AM 1.5G irradiation (100 mW/cm$^2$). In addition, to further examine the universality of the class of polymeric materials as ETM in such perovskite solar cells, two other polymers PNVT-8[33] and PNDI2OD-TT[34] have also been investigated with the same device configuration and decent device performances are obtained as well (PCE 7.47%, and 6.47%, respectively). The model organic small molecule PCBM is used to fabricate the reference devices. As far as we know, this is the first report to introduce organic polymer as ETM in inverted perovskite solar cell since small molecule materials have been used as ETM in perovskite solar cells. We hope this provides a new direction to utilize organic polymers in inverted perovskite solar cell to improve this photovoltaic technique.

## 2. RESULTS AND DISCUSSION

Inverted planar heterojunction perovskite solar cell configuration: ITO/PEDOT:PSS/$CH_3NH_3PbI_{3-x}Cl_x$/Polymer/ZnO/Al (Figure 1a) was employed, with PEDOT:PSS as the HTM, perovskite $CH_3NH_3PbI_{3-x}Cl_x$ as the absorber, polymer as the ETM and aluminum as the cathode. A thin ZnO film (~20 nm) mainly as electron transport layer was applied as it could further improve the device performance. According to the previous reports,[31] the LUMO level of the three polymers are around −3.9 eV, while the HOMO levels are from −5.6 to ~ −5.8 eV, which are similar to the LUMO/HOMO levels of PCBM and matched well with the energy levels of the prepared perovskite $CH_3NH_3PbI_{3-x}Cl_x$, indicating that they can be used as suitable ETMs for this pervoskite solar cell. Together with PEDOT:PSS and electrodes, the energy level alignment was depicted in Figure 2. Perovskite $CH_3NH_3PbI_{3-x}Cl_x$ film was prepared by a one-step procedure according to reference 21. Crystallization of the perovskite film at different annealing temperatures (80, 90, and 100 °C) was investigated separately. Dark brown films were obtained after annealing for 30 min. The optimized result was obtained at an annealing temperature of 90 °C as tetragonal perovskite phase without seeing the $PbI_2$ diffraction peak. The X-ray diffraction (XRD) pattern is shown in Figure 3. The strong diffraction peaks at 14.22 and 28.53° can be assigned to planes (110) and (220) of the $CH_3NH_3PbI_3$


DOI: 10.1021/am506785k
ACS Appl. Mater. Interfaces 2015, 7, 3994−3999

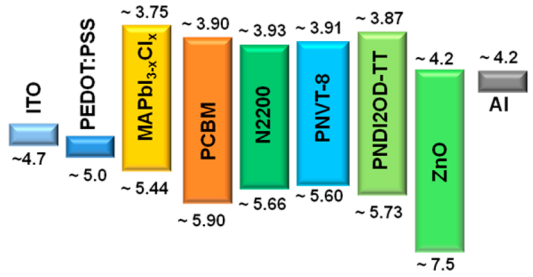


**Figure 2.** Energy level alignment of the materials used in our devices.

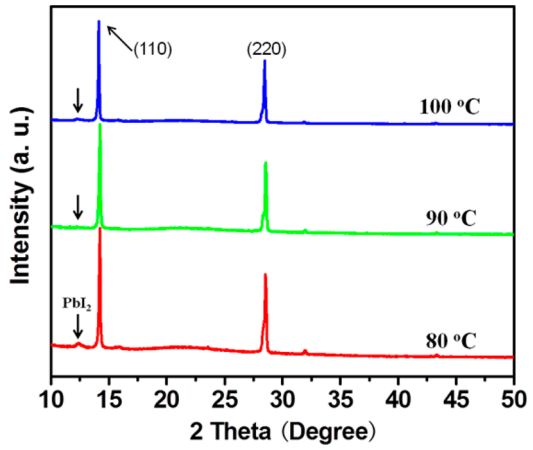


**Figure 3.** XRD patterns of the perovskite films thermal annealed with different temperature.

phase, indicating the formation of perovskite structure. When annealed at a temperature of 80 or 100 °C for 30 min, a weak diffraction peak appears at 12.44°, corresponding to the existence of $PbI_2$. This is consistent with the previous report[35] that at lower temperature, the existence of $PbI_2$ results from the incomplete reaction, while at higher temperature the formation of additional $PbI_2$ is due to the reaction $PbCl_2 + 3CH_3NH_3I \rightarrow PbI_2 + CH_3NH_3I + 2CH_3NH_3Cl$. Thus, the optimal annealing temperature of 90 °C has been applied to all the perovskite devices.

First, with a fixed perovskite layer (around 120 nm), the optimized thickness of the polymeric ETM N2200 was determined to be ~80 nm (Table S1, Supporting Information). Then we fixed this thickness (80 nm) for the N2200 ETM film, and further optimized the perovskite layer again (Table 1). In this way, the best device performance was observed when a 170 nm perovskite film and a ~80 nm N2200 film were used, with a current density ($J_{SC}$) of 14.7 mA/cm$^2$, a $V_{OC}$ of 0.84 V and a fill factor (FF) of 66%, corresponding to PCE of 8.15%. Other perovskite films with thickness decreased or increased (typical 140 and 200 nm) provided lower device performance. In detail, the 140 nm perovskite device provided slightly lowered PCE of 7.18% with reduced $J_{SC}$ of 13.74 mA/cm$^2$. And the 200 nm perovskite delivered a more depressed PCE of 6.61% as the much lowered FF (55%), which could be partially attributed to the increased carrier recombination and/or the rougher interface surface in/of the thick perovskite layer cast by a low spin-coating speed (Figure S1, Supporting Information). For comparison, we fabricated a reference device with PCBM as the ETM with the same architecture and with the same perovskite film thickness (170 nm), which provided better device performance with PCE of 8.51%, as the increased FF 70%, compared to the N2200-based device. Similar results were observed when the perovskite film thickness was changed, but still a bit better than those relative N2200 ETM based device (Table 1). The optimized $J-V$ curves of the devices based on N2200 and PCBM ETM are presented in Figure 4a. In addition, we fabricated a device consisting of the same perovskite film and N2200 film, but without the ZnO layer, which delivered much lower device performance compared to the corresponding device with the ZnO layer (Table 1). We also fabricated a device without either the N2200 or the ZnO layer; however, no working device was obtained (Table S2, Supporting Information). It is worth noting that, occasionally, maximum PCE values of 9.47 and 8.78% were recorded (Table 2) for the PCBM- and N2200 ETM-based devices, respectively, in our experiment. All the above device parameters were recorded with a conventional scan direction from negative to positive bias at a scan rate of 0.1 V s$^{-1}$. Opposite scan direction was also applied to measure the $J-V$ curves to analyze the photocurrent hysteresis properties (Figure S4, Supporting Information) and our perovskite solar cells do not show photocurrent hysteresis.

**Table 1. Photovoltaic Performances of N2200 and PCBM Devices with Different Thickness of Perovskite Film**

| ETM | perovskite thickness (nm) | $J_{SC}$ (mA cm$^{-2}$) | $V_{OC}$ (V) | FF (%) | PCE (%) |
|---|---|---|---|---|---|
| N2200 | 170[a] | 14.23 | 0.80 | 62 | 7.05 |
| | 200[b] | 14.47 | 0.83 | 55 | 6.61 |
| | 170[b] | 14.70 | 0.84 | 66 | 8.15 |
| | 140[b] | 13.74 | 0.83 | 63 | 7.18 |
| PCBM | 200[b] | 14.09 | 0.75 | 67 | 7.08 |
| | 170[b] | 14.65 | 0.83 | 70 | 8.51 |
| | 140[b] | 13.66 | 0.81 | 71 | 7.86 |

[a]ITO/PEDOT:PSS/perovskite/ETM/Al. [b]ITO/PEDOT:PSS/perovskite/ETM/ZnO/Al.

The cross-sectional scanning electron microscope (SEM) images of the optimal devices are shown in Figure 1. The SEM images show that the thickness of the perovskite, PCBM, and N2200 layer is about 170, 60, and 80 nm, respectively. The external quantum efficiency (EQE) measurements were carried out for the optimized devices using N2200 and PCBM ETM respectively. The obtained curves are shown in Figure 4b. The $J_{SC}$ calculated by integrating the EQE curve with an AM 1.5G reference spectrum is within 5% deviation compared to the measured $J_{SC}$. Note that the $J_{SC}$ and $V_{OC}$ obtained from the N2200 and PCBM-based devices are similar and the difference between their PCEs is mainly caused by the different FFs. Considering the tiny difference between the LUMO energy levels of N2200 and PCBM (Figure 2), it should not account much for the low FFs. However, the much lower HOMO level of PCBM compared to N2200 could account for its high FF, to some extent, because it is more effective for hole-blocking. And the much larger series resistance (Table 2) observed for the N2200 device could well explain the low FF.

To sum up, with polymer N2200 as the ETM in the inverted planar heterojunction perovskite solar cell, decent device performances have been delivered, demonstrating that organic polymer N2200 can be an ideal alternative as a new class of ETM in perovskite solar cells.

Moreover, to further demonstrate the universality of organic polymers as a new class of ETM in perovskite solar cells, two other polymers, PNVT-8[33] and PNDI2OD-TT,[34] have also


DOI: 10.1021/am506785k
ACS Appl. Mater. Interfaces 2015, 7, 3994−3999

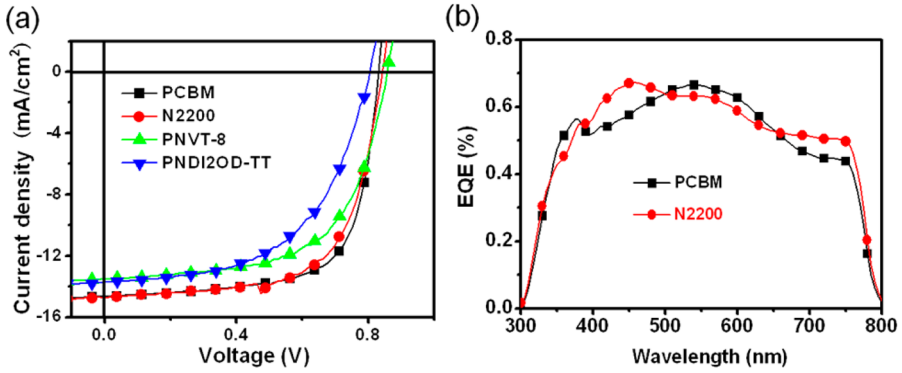


**Figure 4.** (a) $J-V$ characteristics of different ETM-based devices and (b) EQE curves of PCBM and N2200 devices.

**Table 2. Photovoltaic Performances of Inverted Perovskite Solar Cells with Different ETMs**

| ETM | $J_{SC}$ (mA cm$^{-2}$) | $V_{OC}$ (V) | FF (%) | PCE (%)[a] | PCE (%)[b] | $R_S$ (Ω cm$^2$) | $R_{Sh}$ (KΩ cm$^2$) |
|---|---|---|---|---|---|---|---|
| PCBM | 14.65 | 0.83 | 70 | 8.51 | 9.47 | 27.9 | 11.19 |
| N2200 | 14.70 | 0.84 | 66 | 8.15 | 8.78 | 47.6 | 10.58 |
| PNVT-8 | 13.53 | 0.85 | 62 | 7.13 | 7.74 | 57.3 | 11.26 |
| PNDI2OD-TT | 13.71 | 0.81 | 55 | 6.11 | 6.47 | 77.2 | 7.18 |

[a]Average PCEs of inverted perovskite solar cells with different ETMs. [b]Maximum PCEs of inverted perovskite solar cells with different ETMs.

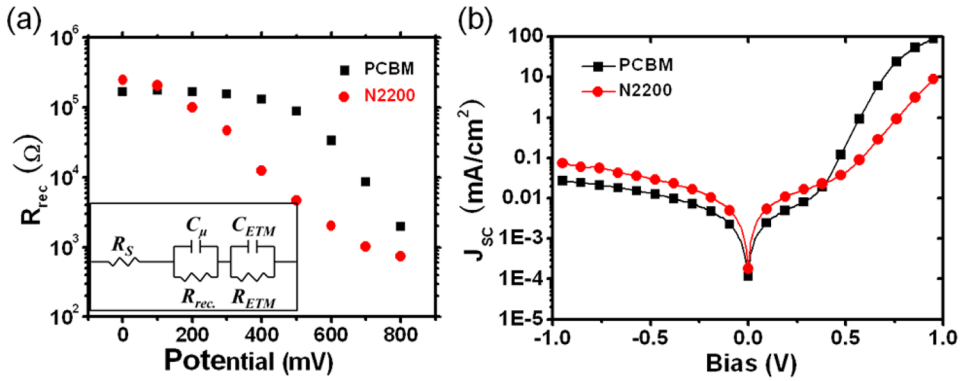


**Figure 5.** (a) Summary of the recombination resistance $R_{rec}$; (inset) simplified equivalent circuit model of the inverted perovskite solar cells. (b) Dark $J-V$ characteristics of N2200 and PCBM devices.

been tested, and fair device performances have been achieved (Table 2) with the similar inverted planar heterojunction configuration. Very similar $J_{SC}$ values were recorded for different ETM-based devices as they employed the same perovskite layer with the same thickness. Compared to N2200, competing $V_{OC}$ values were obtained (Tables 1 and 2), which is consistent with the LUMO energy levels of the polymers (Figure 2), that is close to the LUMO levels of the three polymers would provide similar $V_{OC}$ when combined with the same active material. However, relatively low FFs were recorded, especially for the PNDI2OD-TT ETM based device, resulting in depressed PCE of 7.74 and 6.47%, respectively. Usually, it is complicated to explain for a low FF because many aspects can account for this, like the interface barrier and the carrier recombination rate according to the film quality of different layers, electron mobility, film thickness, and so on. As direct information for evaluating the device, the data of the series and shunt resistance of the devices with ETMs are summarized in Table 2. The lowered FF of the PNVT-8 device is consistent with the increased series resistance. And both the high series resistance and low shunt resistance should account for the lowest FF of the PNDI2OD-TT device, compared to the N2200 one.

To further understand the factors responsible for the low fill factor of the polymer ETM-based solar cells, we experimentally studied the impedance spectroscopy (IS) of the N2200 and PCBM ETM-based devices, for example. The simplified equivalent circuit of the devices is shown in the inset of Figure 5a. Impedance spectra of representative N2200 and PCBM solar cells were recorded at different voltages over the frequency range of 100 Hz to 120 MHz, and the simple equivalent circuit corresponded well with the measurement data throughout the bias voltage range (Figure S2, Supporting Information).

Recombination in PCBM- and N2200-based solar cells was investigated by the change in recombination resistance ($R_{rec}$, which is inversely related to the recombination rate) with voltage, as shown in Figure 5a. The $R_{rec}$ of both perovskite solar cells depends strongly on the bias voltage, following an approximately exponential decrease with voltage, which is in agreement with previous reports.[36−38] The determined $R_{rec}$ of the N2200 device is generally 1 order of magnitude lower than that of the PCBM device, indicating a much faster


DOI: 10.1021/am506785k
ACS Appl. Mater. Interfaces 2015, 7, 3994−3999

recombination rate for N2200 device than the PCBM device, consequently the increased charge carrier recombination, and hence the loss of $J_{SC}$ and FF. However, a very slight increase of $J_{SC}$ was observed compared to the huge decrease in FF; we consider the $J_{SC}$ could have been partially compensated by the carriers generated by the polymer due to its good absorption (Figure S3, Supporting Information). Again, similar results were confirmed in their markedly different dark $J-V$ characteristics, as shown in Figure 5b. The PCBM device exhibits higher rectification ratio and lower leakage current under reverse bias than the N2200 one, as the improved diode characteristics due to the larger parallel resistance and lower serial resistance.

## 3. CONCLUSIONS

We report the application of polymer N2200, PNVT-8, and PNDI2OD-TT as ETM in inverted planar heterojunction perovskite solar cells in this work. Decent and competitive device performance with average parameters of $J_{SC}$ 14.7 mA/cm$^2$, $V_{OC}$ 0.84 V, FF 66%, and PCE ~8.15% was achieved for the ideal N2200 ETM-based device, compared to the parameters ($J_{SC}$ 14.65 mA/cm$^2$, $V_{OC}$ 0.83 V, FF 70%, and PCE 8.51%) of the reference device employing model organic small molecule PCBM as ETM. Decent device parameters were obtained for the PNVT-8 and PNDI2OD-TT ETM based devices as well. We consider that the tiny difference in LUMO levels of the polymers compared to the PCBM should mainly account for their similar $V_{OC}$ values, and the much lower HOMO level of PCBM should partly account for its high FF. Moreover, the IS investigations demonstrated that the N2200 device possess a much lower recombination resistance than the PCBM device does, which should mainly account for its low FF. We hope this work will provide new direction to utilize organic polymers as a new class of ETM in inverted perovskite solar cell to further promote this technique.

## 4. EXPERIMENTAL SECTION

**4.1. Materials Synthesis.** All chemicals, unless otherwise noted, were purchased from Alfa or J&K Chemicals, and then used as received. Colloidal ZnO nanocrystals were synthesized according to literature procedures.[9] Polymers (N2200, PNVT-8, and PNDI2OD-TT) were prepared according to previous studies.[33,34] $CH_3NH_3I$ was synthesized with the modified method published in literature.[1]

**4.2. Device Fabrication.** Precleaned indium–tin oxide (ITO) substrates were treated with ultraviolet-ozone (UVO) for 20 min. Then, the poly(3,4-ethylene-dioxy-thiophene):polystyrene (PEDOT:PSS) were spin-coated on the ITO substrates at 4500 rpm for 40 s and baked at 150 °C for 10 min in atmosphere. The deposition of the other layers including perovskite layer, ETMs, ZnO layer and the cathode electrode were finished in the $N_2$ glovebox ($H_2O$: <1 ppm and $O_2$: <1 ppm). In detail, a 30 wt % $CH_3NH_3PbI_{3-x}Cl_x$ precursor solution (which was prepared by dissolving $CH_3NH_3I$ and $PbCl_2$ in anhydrous DMF at a molar ratio of 3:1, and stirred at 60 °C for 12 h) was spin-coated on the PEDOT:PSS layer at different speeds (2000, 3000, and 4000 rpm) for 40 s. Then the perovskite films were annealed on a hot plate at 90 °C for ~30 min, by which the color of the films converted from yellow to brown. After being cooled to room temperature, the ETM layers were deposited onto the perovskite film by spin-coating with their corresponding chlorobenzene solution (5 mg/mL for polymers, 30 mg/mL for PCBM). Subsequently, the ZnO layers were formed by spin-coating a colloidal ZnO nanocrystal solution (6 mg/mL) at 3000 rpm for 30s. Finally, the 100 nm-thick Al cathode was formed by thermal vacuum evaporation through a shadow mask (active area 7.25 mm$^2$) under $10^{-6}$ Torr (Mini-SPECTROS, Kurt J. Lesker Co.). The current density–voltage ($J-V$) parameters of the devices were characterized by using a Keithley 2400 digital source meter at dark or under simulated AM 1.5G solar irradiation at 100 mW/cm$^2$ (Newport, Class AAA solar simulator, 94023A-U). The light intensity was calibrated by a certified Oriel Reference Cell (91150 V) and verified with an NREL calibrated Hamamatsu S1787–04 diode. The EQE was performed using a certified IPCE instrument (Zolix Instruments, Inc., Solar Cell Scan 100).

**4.3. Characterization.** The photoluminescence (PL) measurements were carried out on a FluoroMax-4 Spectrofluorometer (HORIBA Scientific). SEM images were obtained from a field emission scanning electron microscope (FEI Quanta 200). The ultraviolet–visible spectroscopy (UV–vis) spectra were recorded on a PerkinElmer model Lambda 750 instrument. Conventional XRD measurement was conducted using a PANalytical (Empyrean) equipment. In the characterizations, the needed layers in samples were prepared just following the device fabrication procedure. For optical and XRD measurements, the perovskite films were sealed by spin-coating a layer of poly(methyl methacrylate) (PMMA) on top. The impedance spectroscopy (IS) measurements were taken by a Wayne Kerr 6550B precision impedance analyzer in a frequency range from 100 Hz to 120 MHz, with a 15 mV perturbation oscillation signal.

## ■ ASSOCIATED CONTENT

### Ⓢ Supporting Information

SEM images of $CH_3NH_3PbI_{3-x}Cl_x$ perovskite film with different thickness, representative Nyquist plots, absorption and steady-state PL, photocurrent hysteresis, photovoltaic performances of inverted perovskite solar cells with different thickness of ETMs (N2200), different device configuration, different ETM with or without ZnO layer. This material is available free of charge via the Internet at http://pubs.acs.org.

## ■ AUTHOR INFORMATION

### Corresponding Authors

*E-mail: whqbme@gmail.com.
*E-mail: wlma@suda.edu.cn.

### Notes

The authors declare no competing financial interest.

## ■ ACKNOWLEDGMENTS

This work was supported by the National High Technology Research and Development Program of China (863 Program, Grant No. 2011AA050520), the National Natural Science Foundation of China (Grant No. 61176054), the Natural Science Foundation of Jiangsu Province (No. BK20130311), and the Postdoctoral Science Foundation (Grant Nos. 2014M550302 and 1302015A). And we also acknowledge the Collaborative Innovation Center of Suzhou Nano Science and Technology, the Priority Academic Program Development of Jiangsu Higher Education Institutions (PAPD).

## ■ REFERENCES

(1) Kim, H. S.; Lee, C. R.; Im, J. H.; Lee, K. B.; Moehl, T.; Marchioro, A.; Moon, S. J.; Humphry-Baker, R.; Yum, J. H.; Moser, J. E.; Gratzel, M.; Park, N. G. Lead Iodide Perovskite Sensitized All-Solid-State Submicron Thin Film Mesoscopic Solar Cell with Efficiency Exceeding 9%. *Sci. Rep.* **2012**, *2* (591), 1–7.

(2) Im, J.-H.; Lee, C.-R.; Lee, J.-W.; Park, S.-W.; Park, N.-G. 6.5% Efficient Perovskite Quantum-Dot-Sensitized Solar Cell. *Nanoscale* **2011**, *3*, 4088–4093.

(3) Kim, H. S.; Im, S. H.; Park, N. G. Organolead Halide Perovskite: New Horizons in Solar Cell Research. *J. Phys. Chem. C* **2014**, *118*, 5615–5625.

(4) Stranks, S. D.; Eperon, G. E.; Grancini, G.; Menelaou, C.; Alcocer, M. J. P.; Leijtens, T.; Herz, L. M.; Petrozza, A.; Snaith, H. J. Electron-Hole Diffusion Lengths Exceeding 1 Micrometer in an



DOI: 10.1021/am506785k
*ACS Appl. Mater. Interfaces* 2015, 7, 3994–3999

Organometal Trihalide Perovskite Absorber. *Science* **2013**, *342*, 341−344.
(5) Xing, G.; Mathews, N.; Sun, S.; Lim, S. S.; Lam, Y. M.; Gratzel, M.; Mhaisalkar, S.; Sum, T. C. Long-Range Balanced Electron- and Hole-Transport Lengths in Organic−Inorganic $CH_3NH_3PbI_3$. *Science* **2013**, *342*, 344−347.
(6) Heo, J. H.; Im, S. H.; Noh, J. H.; Mandal, T. N.; Lim, C. S.; Chang, J. A.; Lee, Y. H.; Kim, H. J.; Sarkar, A.; Nazeeruddin, M. K.; Gratzel, M.; Seok, S. I. Efficient Inorganic-organic Hybrid Heterojunction Solar Cells Containing Perovskite Compound and Polymeric Hole Conductors. *Nat. Photonics* **2013**, *7*, 487−492.
(7) Burschka, J.; Pellet, N.; Moon, S. J.; Humphry-Baker, R.; Gao, P.; Nazeeruddin, M. K.; Gratzel, M. Sequential Deposition as a Route to High-Performance Perovskite-Sensitized Solar Cells. *Nature* **2013**, *499*, 316−319.
(8) Liu, M.; Johnston, M. B.; Snaith, H. J. Efficient Planar Heterojunction Perovskite Solar Cells by Vapour Deposition. *Nature* **2013**, *501*, 395−398.
(9) Liu, D.; Kelly, T. L. Perovskite Solar Cells With a Planar Heterojunction Structure Prepared Using Room-Temperature Solution Processing Techniques. *Nat. Photonics* **2013**, *8*, 133−138.
(10) Malinkiewicz, O.; Yella, A.; Lee, Y. H.; Espallargas, G. M.; Graetzel, M.; Nazeeruddin, M. K.; Bolink, H. J. Perovskite Solar Cells Employing Organic Charge-Transport Layers. *Nat. Photonics* **2014**, *8*, 128−132.
(11) Kojima, A.; Teshima, K.; Shirai, Y.; Miyasaka, T. Organometal Halide Perovskites as Visible-Light Sensitizers for Photovoltaic Cells. *J. Am. Chem. Soc.* **2009**, *131*, 6050−6051.
(12) Wang, J. T.; Ball, J. M.; Barea, E. M.; Abate, A.; Alexander-Webber, J. A.; Huang, J.; Saliba, M.; Mora-Sero, I.; Bisquert, J.; Snaith, H. J.; Nicholas, R. J. Low-temperature Processed Electron Collection Layers of Graphene/$TiO_2$ Nanocomposites in Thin Film Perovskite Solar Cells. *Nano Lett.* **2014**, *14*, 724−730.
(13) Abate, A.; Saliba, M.; Hollman, D. J.; Stranks, S. D.; Wojciechowski, K.; Avolio, R.; Grancini, G.; Petrozza, A.; Snaith, H. J. Supramolecular Halogen Bond Passivation of Organic−Inorganic Halide Perovskite Solar Cells. *Nano Lett.* **2014**, *14*, 3247−3254.
(14) Wojciechowski, K.; Saliba, M.; Leijtens, T.; Abate, A.; Snaith, H. Sub 150 °C Processed Meso-Superstructured Perovskite Solar Cells with Enhanced Efficiency. *Energy Environ. Sci.* **2013**, *7*, 1142−1147.
(15) Lee, J.-W.; Seol, D.-J.; Cho, A.-N.; Park, N.-G. High-Efficiency Perovskite Solar Cells Based on the Black Polymorph of $HC(NH_2)_2PbI_3$. *Adv. Mater.* **2014**, *26*, 4991−4998.
(16) Jeon, N. J.; Lee, H. G.; Kim, Y. C.; Seo, J.; Noh, J. H.; Lee, J.; Seok, S. I. *o*-Methoxy Substituents in Spiro−OMeTAD for Efficient Inorganic−Organic Hybrid Perovskite Solar Cells. *J. Am. Chem. Soc.* **2014**, *136*, 7837−7840.
(17) Jeon, N. J.; Noh, J. H.; Kim, Y. C.; Yang, W. S.; Ryu, S.; Seok, S. I. Solvent Engineering for High-performance Inorganic−Organic Hybrid Perovskite Solar Cells. *Nat. Mater.* **2014**, *13*, 897−903.
(18) Zhou, H.; Chen, Q.; Li, G.; Luo, S.; Song, T. b.; Duan, H. S.; Hong, Z.; You, J.; Liu, Y.; Yang, Y. Interface Engineering of Highly Efficient Perovskite Solar Cells. *Science* **2014**, *345*, 542−546.
(19) Lee, M. M.; Teuscher, J.; Miyasaka, T.; Murakami, T. N.; Snaith, H. J. Efficient Hybrid Solar Cells Based on Meso-Superstructured Organometal Halide Perovskites. *Science* **2012**, *338*, 643−647.
(20) Jeng, J. Y.; Chiang, Y. F.; Lee, M. H.; Peng, S. R.; Guo, T. F.; Chen, P.; Wen, T. C. $CH_3NH_3PbI_3$ Perovskite/Fullerene Planar−Heterojunction Hybrid Solar Cells. *Adv. Mater.* **2013**, *25*, 3727−3732.
(21) Docampo, P.; Ball, J. M.; Darwich, M.; Eperon, G. E.; Snaith, H. J. Efficient Organometal Trihalide Perovskite Planar−Heterojunction Solar Cells on Flexible Polymer Substrates. *Nat. commun.* **2013**, *4*, 2761.
(22) Sun, S.; Salim, T.; Mathews, N.; Duchamp, M.; Boothroyd, C.; Xing, G.; Sum, T. C.; Lam, Y.-M. The Origin of High Efficiency in Low-Temperature Solution-Processable Bilayer Organometal Halide Hybrid Solar Cells. *Energy Environ. Sci.* **2013**, *7*, 399−407.
(23) Seo, J. W.; Park, S.; Kim, Y. C.; Jeon, N. J.; Noh, J. H.; Yoon, S. C.; Seok, S. I. Benefits of Very Thin PCBM and LiF Layer for Solution-Processed P-I-N Perovskite Solar Cells. *Energy Environ. Sci.* **2014**, *7*, 2642−2646.
(24) Liang, P.-W.; Liao, C.-Y.; Chueh, C.-C.; Zuo, F.; Williams, S. T.; Xin, X.-K.; Lin, J.; Jen, A. K. Y. Additive Enhanced Crystallization of Solution-Processed Perovskite for Highly Efficient Planar-Heterojunction Solar Cells. *Adv. Mater.* **2014**, *26*, 3748−3754.
(25) Zuo, C.; Ding, L. An 80.11% FF Record Achieved for Perovskite Solar Cells by Using the NHCl Additive. *Nanoscale* **2014**, *6*, 9935−9938.
(26) Kim, H.-B.; Choi, H.; Jeong, J.; Kim, S.; Walker, B.; Song, S.; Kim, J. Y. Mixed Solvents for the Optimization of Morphology in Solution-Processed, Inverted-type Perovskite/Fullerene Hybrid Solar Cells. *Nanoscale* **2014**, *6*, 6679−6683.
(27) Hsu, H. L.; Chen, C. P.; Chang, J. Y.; Yu, Y. Y.; Shen, Y. K. Two-Step Thermal Annealing Improves the Morphology of Spin-Coated Films for Highly Efficient Perovskite Hybrid Photovoltaics. *Nanoscale* **2014**, *6*, 10281−10288.
(28) Barrows, A.; Pearson, A.; Kwak, C.; Dunbar, A.; Buckley, A.; Lidzey, D. Efficient Planar Heterojunction Mixed-Halide Perovskite Solar Cells Deposited via Spray-Deposition. *Energy Environ. Sci.* **2014**, *7*, 2944−2950.
(29) Xiao, Z.; Bi, C.; Shao, Y.; Dong, Q.; Wang, Q.; Yuan, Y.; Wang, C.; Gao, Y.; Huang, J. Efficient, High-Yield Perovskite Photovoltaic Devices Grown by Interdiffusion of Solution-Processed Precursor Stacking Layers. *Energy Environ. Sci.* **2014**, *7*, 2619.
(30) Chiang, C. H.; Tseng, Z. L.; Wu, C. G. Planar Heterojunction Perovskite/PC71BM Solar Cells with Enhanced Open-Circuit Voltage via a (2/1)-Step Spin-Coating Process. *J. Mater. Chem. A* **2014**, *2*, 15897−15903.
(31) Yan, H.; Chen, Z.; Zheng, Y.; Newman, C.; Quinn, J. R.; Dotz, F.; Kastler, M.; Facchetti, A. A High-Mobility Electron-Transporting Polymer for Printed Transistors. *Nature* **2009**, *457*, 679−686.
(32) Chen, Z.; Zheng, Y.; Yan, H.; Facchetti, A. Naphthalenedicarboximide- vs Perylenedicarboximide-Based Copolymers. Synthesis and Semiconducting Properties in Bottom-Gate N-Channel Organic Transistors. *J. Am. Chem. Soc.* **2008**, *131*, 8−9.
(33) Chen, H.; Guo, Y.; Mao, Z.; Yu, G.; Huang, J.; Zhao, Y.; Liu, Y. Naphthalenediimide-Based Copolymers Incorporating Vinyl-Linkages for High-Performance Ambipolar Field-Effect Transistors and Complementary-Like Inverters under Air. *Chem. Mater.* **2013**, *25*, 3589−3596.
(34) Luzio, A.; Fazzi, D.; Natali, D.; Giussani, E.; Baeg, K.-J.; Chen, Z.; Noh, Y.-Y.; Facchetti, A.; Caironi, M. Synthesis, Electronic Structure, and Charge Transport Characteristics of Naphthalenediimide-Based Co-Polymers with Different Oligothiophene Donor Units. *Adv. Funct. Mater.* **2014**, *24*, 1151−1162.
(35) Dualeh, A.; Tetreault, N.; Moehl, T.; Gao, P.; Nazeeruddin, M. K.; Gratzel, M. Effect of Annealing Temperature on Film Morphology of Organic−Inorganic Hybrid Pervoskite Solid-State Solar Cells. *Adv. Funct. Mater.* **2014**, *24*, 3250−3258.
(36) Christians, J. A.; Fung, R. C.; Kamat, P. V. An Inorganic Hole Conductor for Organo-Lead Halide Perovskite Solar Cells. Improved Hole Conductivity with Copper Iodide. *J. Am. Chem. Soc.* **2014**, *136*, 758−764.
(37) Kim, H. S.; Mora-Sero, I.; Gonzalez-Pedro, V.; Fabregat-Santiago, F.; Juarez-Perez, E. J.; Park, N. G.; Bisquert, J. Mechanism of Carrier Accumulation in Perovskite Thin-Absorber Solar Cells. *Nat. Commun.* **2013**, *4*, 2242.
(38) Zhao, Y.; Zhu, K. $CH_3NH_3Cl$-Assisted One-Step Solution Growth of $CH_3NH_3PbI_3$: Structure, Charge-Carrier Dynamics, and Photovoltaic Properties of Perovskite Solar Cells. *J. Phys. Chem. C* **2014**, *118*, 9412−9418.


DOI: 10.1021/am506785k
*ACS Appl. Mater. Interfaces* 2015, 7, 3994−3999